

Power spectrum normalization from the local abundance of rich clusters of galaxies

Elena Pierpaoli¹, Douglas Scott¹ and Martin White²

¹*Department of Physics and Astronomy, University of British Columbia, BC V6T1Z1 Canada*

²*Harvard-Smithsonian Center for Astrophysics, Cambridge, MA 02138*

Accepted ... ; Received ... ; in original form ...

ABSTRACT

The number density of rich galaxy clusters still provides the most robust way of normalizing the power spectrum of dark matter perturbations on scales relevant to large-scale structure. We revisit this constraint in light of several recent developments: (1) the availability of well-defined samples of local clusters with relatively accurate X-ray temperatures; (2) new theoretical mass functions for dark matter haloes which provide a good fit to large numerical simulations; (3) more accurate mass-temperature relations from larger catalogues of hydrodynamical simulations; (4) the requirement to consider closed as well as open and flat cosmologies to obtain full multi-parameter likelihood constraints for CMB and SNe studies. We present a new sample of clusters drawn from the literature and use this sample to obtain improved results on σ_8 , the normalization of the matter power spectrum on scales of $8 h^{-1}$ Mpc, as a function of the matter density and cosmological constant in a Universe with general curvature. We discuss our differences with previous work, and the remaining major sources of uncertainty. Final results on the normalization, approximately independent of power spectrum shape, can be expressed as constraints on σ at an appropriate cluster normalization scale R_{Cl} . We provide fitting formulas for R_{Cl} and $\sigma(R_{\text{Cl}})$ for general cosmologies, as well as for σ_8 as a function of cosmology and shape parameter Γ . For flat models we find approximately $\sigma_8 \simeq (0.495^{+0.034}) \Omega_M^{-0.60}$ for $\Gamma = 0.23$, where the error bar is dominated by uncertainty in the mass-temperature relation.

Key words: cosmology: theory – large-scale structure of Universe – galaxies: clusters – X-rays

1 INTRODUCTION

In theories of hierarchical structure formation the class of objects most recently formed holds a special significance. Observationally this class of objects is clusters of galaxies – the largest virialized structures in the present day universe. The local abundance of rich clusters of galaxies provides a strong constraint on the fluctuations in the matter density on scales of order 10 Mpc (Evrard 1989; Frenk et al. 1990; Kaiser 1991; Bond & Myers 1991; Lilje 1992; Oukbir & Blanchard 1992; Hanry & Arnaud 1991; Bahcall & Cen 1993; Hanami 1993; White, Efstathiou & Frenk 1993). Consistency with this constraint is one of the most important tests a model can pass, since the constraint is directly on the linear theory power spectrum, at a scale where there is an abundance of data. By fixing the normalization at wavelengths much smaller than those probed by COBE one obtains an accurate local normalization on scales relevant to much of structure formation, a long lever arm for constrain-

ing the shape of the power spectrum, and a normalization to matter fluctuations which is independent of galaxy bias.

There have been several recent and detailed studies of the cluster abundance, including Eke, Cole & Frenk (1996), Eke et al. (1998), Viana & Liddle (1996; 1999), Bond & Myers (1996), Kitayama & Suto (1997), Wang & Steinhardt (1998), Colafrancesco, Mazzotta & Vittorio (1997) and Pen (1998). However, even more recently, there have been several developments in terms of both theory and observation which suggest it would be useful to revisit this constraint. Firstly the addition of ASCA temperatures (Tanaka, Inoue & Holt 1994) means that there is now a well defined local temperature function for clusters, with relatively small errors in temperature. Secondly a number of large N-body simulations have accurately determined the mass function of virialized haloes (e.g. Governato et al. 1999), finding non-negligible deviations from the old Press-Schechter (1974; hereafter PS) theory. For example the extremely large N-body simulations of the Virgo consortium have highlighted systematic departures from the PS predicted mass functions (Jenkins et al.

2000), which alter the constraints on the power spectrum normalization coming from the cluster abundance. Thirdly, more ambitious hydrodynamical simulations of cluster formation (e.g. Frenk et al. 1999, and references therein) have resulted in improvements in the relationship between mass and temperature and a better estimate of its scatter. Finally, the increased sophistication of multi-parameter cosmological studies (in particular driven by recent CMB anisotropy measurements) requires that cosmological models with general curvature be considered.

With these refinements our results are an improvement over other studies of the past few years. We point out explicitly where we differ from other work, and also where we think things could be further improved in the future. The outline of the paper is as follows: we review some of the appropriate theory in §2; our local sample of clusters is presented in §3; we describe our statistical method in §4; and we present our results and conclusions in §5 and §6.

2 THEORY

The abundance of rich clusters is tied to the normalization of the power spectrum (extrapolated to the present using linear theory) through the Press-Schechter (1974) theory and its extensions (see Sheth, Mo & Tormen 2000 and references therein). The theory has always had a somewhat weak analytic justification, its widespread adoption arising from the dual facts that it is easy to use and provides a remarkably good fit to more computationally expensive simulations.

Although galaxy velocity dispersion and gravitational lensing mass estimates exist for many clusters (Girardi et al. 1998; Allen 1998), the direct estimation of mass through determination of the X-ray temperature is by far the most reliable – although the situation is certainly improving, allowing for estimates of the mass function (Girardi et al. 1998b; Borgani et al. 1999). In the X-ray band there is considerably more high quality data on luminosity than on temperature, but there is enormous uncertainty in deriving mass M from luminosity L_X . Hence the point of comparison between theory and observation will be the temperature function of rich clusters, i.e. the number density of clusters within a temperature range dT about T . This needs to be observationally determined over some range of T sufficiently high that gravitational physics dominates. Observational and theoretical considerations place this limit at $T_X \gtrsim 3.5$ keV (e.g. Finoguenov et al. 2000; Nevalainen, Markevitch & Forman 2000). Ideally we could compare the data with a temperature function estimated directly from a series of large cosmological hydrodynamic simulations (see e.g. Pen 1998), which included all of the physics relevant to determining the emission weighted inter-galactic medium (IGM) temperature of clusters. This however is currently computationally infeasible. Instead we shall make use of the fact that rich clusters are large virialized structures dominated by gravity, and thus we can factorize the problem and proceed in two steps.

First we shall use the abundance of dark matter haloes of a given mass drawn from extremely large N-body simulations. Any dark matter halo large enough to host a cluster is unambiguously seen in such simulations. Next we shall use a mass-temperature relation, calibrated from hydrodynamical simulations, to convert from the (unobservable) virial mass

to the IGM temperature, effectively using the larger volume of the N-body simulations to improve the statistics of the hydro simulations. Unfortunately the mass functions determined from the N-body simulations are somewhat dependent on the method used to define haloes and their masses, and the precise definition of mass is not exactly what is used in the hydrodynamic simulations which calibrate the $M-T$ relation; the difference is expected to be small however (Jenkins et al. 2000). We discuss further details of the $M-T$ relation in §§2.4 and 2.5.

2.1 The mass variance

Our constraint will be on the variance of the density field, smoothed on some (comoving) scale R corresponding to a mass $M = (4\pi/3)\bar{\rho}R^3$ where $\bar{\rho}$ is the background density. In terms of the power spectrum

$$\sigma^2(R, z) = \int_0^\infty \frac{dk}{k} \Delta^2(k, z) W^2(kR), \quad (1)$$

where $\Delta^2 = k^3 P(k, z)/(2\pi^2)$, $P(k) \equiv |\delta_k|^2$ is the matter power spectrum and $W(kR)$ is the window function corresponding to the smoothing of the density field (see e.g. Peebles 1993). Our mass functions are fitted assuming a spherical top-hat smoothing, so

$$W(kR) = \left(\frac{3j_1(kR)}{kR} \right), \quad (2)$$

where $j_1(x)$ is the spherical Bessel function of order 1. We are interested in both the normalization of the power spectrum, for which we shall use $\sigma_8 \equiv \sigma(8h^{-1}\text{Mpc})$, and its shape. We use the Cold Dark Matter family of power spectra and parameterize the shape by Γ in the fitting formula of Bardeen et al. (1986). While the form of Eisenstein & Hu (1999) provides a slightly better fit to the shape, we will quote the results in a Γ independent way, rendering this distinction unimportant.

We write $\sigma(R, z) = g(z)/g(0)\sigma(R, 0)$ where the growth factor $g(z)$ can be computed numerically (Heath 1977; Carroll, Press & Turner 1992; Cohn 1999; Carroll 2000; Hamilton 2000):

$$g(z) = \frac{5\Omega_M}{2} \frac{da}{a} \int_0^a da' \left(\frac{da'}{d\tau} \right)^{-3}, \quad (3)$$

where the scale factor $a = (1+z)^{-1}$, and the dimensionless time $\tau \equiv H_0 t$. The Friedmann equation gives

$$\left(\frac{\dot{a}}{a} \right)^2 = H_0^2 \left(\frac{\Omega_M}{a^3} + \Omega_\Lambda + \frac{\Omega_K}{a^2} \right), \quad (4)$$

where $H_0 \equiv (\dot{a}/a)_0$ is the Hubble constant. The usual symbols Ω_M , $\Omega_\Lambda \equiv \Lambda/3H_0^2$ and $\Omega_K \equiv 1 - \Omega_M - \Omega_\Lambda$ are the density parameters (ρ/ρ_{crit} , with $\rho_{\text{crit}} = 3H_0^2/8\pi G$) in matter, cosmological constant and curvature, respectively. Photons and other relativistic species can be safely ignored.

2.2 Press-Schechter and modifications

Within the PS theory and its extensions the (comoving) number density of objects of (virial) mass M is a function only of $\sigma(M)$. Using the scaled variable

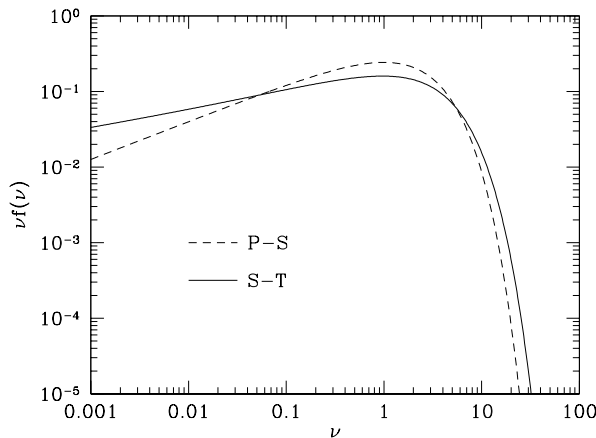


Figure 1. A comparison of the Press-Schechter form for the multiplicity function, used in all previous work, with the Sheth & Tormen (1999) model, which better fits the Virgo simulation results (see text). Note that Press-Schechter systematically underestimates the abundance of the most massive cluster haloes, $\nu \sim 10$, and can either overestimate or underestimate the abundance of more typical clusters with $\nu \sim$ few.

$$\nu \equiv \left(\frac{\delta_c}{\sigma(M)} \right)^2 \quad (5)$$

with $\delta_c \equiv 1.686$ we write the mass function in terms of the ‘multiplicity function’ $f(\nu)$ as

$$\nu f(\nu) = \frac{M^2}{\bar{\rho}} \frac{dn}{dM} \frac{d\ln M}{d\ln \nu}. \quad (6)$$

In the spirit of using PS as a fitting function to N-body simulations we do not imbue δ_c with a cosmology dependence (see next section) but rather keep it constant. The Press-Schechter model for $f(\nu)$ is

$$\nu f(\nu) = \sqrt{\frac{\nu}{2\pi}} e^{-\nu/2}, \quad (7)$$

and this formula has been extensively used to make predictions on cluster abundances in different cosmologies. Recently Sheth & Tormen (1999) have proposed a correction to the Press-Schechter formula, motivated by a model of non-spherical collapse, that better fits large N-body simulations:

$$\nu f(\nu) \propto (1 + \tilde{\nu}^{-p}) \tilde{\nu}^{1/2} e^{-\tilde{\nu}/2}, \quad (8)$$

where $p = 0.3$ and $\tilde{\nu} = 0.707\nu$. The normalization constant is fixed by the requirement that all of the mass be in haloes, i.e.

$$\int f(\nu) d\nu = 1; \quad (9)$$

for the above choice of parameters the normalization factor is 0.2162. Jenkins et al. (2000) have shown that Eq. (8) is in very good agreement with the simulations of the Virgo Consortium except for very rare objects which shall not be of interest in this work. We compare the multiplicity functions in Fig. 1. Note that Press-Schechter systematically overestimates the abundance of objects of cluster mass having $1 \gtrsim \nu \gtrsim 6$ ($\sigma(R) \lesssim 0.7$) and underestimates the abundance of objects corresponding to a higher $\sigma(R)$.

i	j				
	0	1	2	3	4
0	352.2	98.46	68.44	-111.5	41.38
1	-628.0	-556.2	-621.0	1101.	-481.0
2	1120.	1660.	1143.	-2649.	1262.
3	-1112.	-2215.	-612.3	2442.	-1267.
4	438.5	1026.	37.59	-819.8	463.3

Table 1. Coefficients c_{ij} of the fitting formula, Eq. (10), for the collapse overdensity Δ_c .

2.3 Spherical top-hats

The spherical top-hat ansatz (Peebles 1993; Liddle & Lyth 2000; Peacock 1999) models the formation of an object by the evolution of a spherical overdense region embedded in a homogeneous ‘background’ of mean density $\bar{\rho}$. This begins by expanding at the same rate as the background, but since it is positively curved this expansion slows, comes to a halt and the region collapses. Mathematically the evolution proceeds to a point of zero radius, however physically we assume that virialization occurs at twice* the turn-around time, resulting in a sphere of half the turn-around radius. The overdensity (relative to the background) at turn-around is $9\pi^2/16$ for an Einstein-de Sitter model. At virialization the background has become less dense and the sphere’s density grown by a further factor of 8 – we then denote the overdensity relative to the critical density by Δ_c . This parameter has the value $18\pi^2$ in an Einstein-de Sitter model, and will in general be a function of Ω_M and Ω_Λ . The extrapolation from linear theory of this overdensity is normally denoted δ_c . It is $(3/20)(12\pi)^{2/3} \simeq 1.686$ for Einstein-de Sitter and varies by a few percent in other cosmologies. This density is used as a threshold in PS theory and its extensions. We shall neglect the small cosmology dependence and simply take δ_c fixed throughout.

The value of the density contrast at collapse, Δ_c , on the other hand, should be calculated each model, since it will be important for the $M-T$ relation. We computed Δ_c by numerically integrating the equations of motion for the spherical top-hat collapse, including the correction to the virial theorem from the Λr^2 potential (Lahav et al. 1991; §4.2). Our results can be fit to 2 per cent over the range $0.2 \leq \Omega_M \leq 1.1$ and $0 \leq \Omega_\Lambda \leq 1$ by

$$\Delta_c = \Omega_M \sum_{i,j=0}^4 c_{ij} x^i y^j, \quad (10)$$

where $x \equiv \Omega_M - 0.2$, $y \equiv \Omega_\Lambda$ and the coefficients c_{ij} are reported in Table 1. As an example we plot Δ_c vs Ω_M for flat models, where the dashed line shows our fit and the solid line is the exact relation. We also checked this fit with the one provided by Eke, Navarro & Frenk (1998) and found an agreement at the 1 per cent level. Note that some authors use a different convention in which Δ_c is specified relative to the background matter density – our Δ_c is Ω_M times theirs.

* In the presence of a cosmological constant there is a small modification to this.

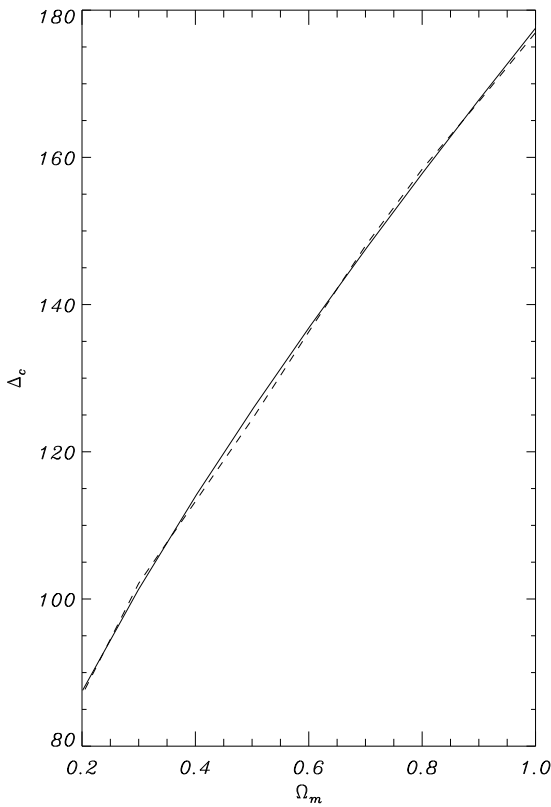


Figure 2. Showing our fit to the overdensity at virialization, Δ_c vs Ω_M for flat models, where the dashed curve is our fitting function and the solid curve is the exact result.

2.4 Halo mass definitions

Before we turn to the mass-temperature relation we note a few important details about determining the mass of a dark-matter halo. Unfortunately there is no unique algorithmic definition of a dark matter halo, even within a 3D simulation itself. Some group finders are in common use, but no single group finder is always used. For large objects such as clusters all group finders should be able to find all of the clusters so this is not of immediate concern, though the degree of substructure will be highly variable between group finders.

More disconcertingly there are a wide number of definitions of halo *mass* in the literature, and they can differ by a large amount. Even for the mass-temperature relations calibrated by hydro simulations different authors use different definitions of ‘mass’, with the differences dependent on the cosmological parameters. In this sub-section we briefly review the relevant mass definitions and discuss which is the most appropriate for the mass function of Eq. (8).

Although other halo finders are in common use, we shall deal exclusively with haloes found using the Friends-of-Friends (Davis et al. 1985) algorithm, hereafter called FOF. The FOF algorithm has one free parameter, b , the linking length in units of the mean inter-particle spacing. Commonly used values of b are 0.1, 0.15 and 0.2. The mass of the halo is simply the sum of the masses of the particles identified as part of the halo. An alternative (and more easily inter-

preted) procedure is to use FOF to find candidate haloes, identify a halo centre (e.g. the centre of mass of the halo or, more robustly, the position of the most bound particle) and then to calculate the mass from the spherically averaged density profile about that centre. This is the technique typically used to define the mass in hydrodynamic simulations which calibrate the $M - T$ relation.

In this spirit we define M_Δ as the mass contained within a radius r_Δ , inside of which the mean interior density is Δ times the *critical* density:

$$\int_0^{r_\Delta} r^2 dr \rho(r) = \frac{\Delta}{3} \rho_{\text{crit}} r_\Delta^3. \quad (11)$$

The ‘virial mass’ from the spherical top-hat collapse model would then be simply M_{Δ_c} . Other masses in common use are M_{500} and M_{200} where the latter is approximately the virial mass if $\Omega_M = 1$.

For large mass haloes many of these definitions are related on average simply by a factor. We can estimate this factor by assuming that haloes have a universal profile, for example the NFW form (Navarro, Frenk & White 1996):

$$\rho(r) \propto x^{-1} (1+x)^{-2}, \quad (12)$$

where $x = r/r_s$ and r_s is a scale radius usually specified in terms of the concentration parameter $c \equiv r_{200}/r_s$. Navarro et al. (1996) refer to r_{200} and M_{200} throughout as the ‘virial radius’ and ‘virial mass’ respectively. Again, N-body simulations have shown that the concentration parameter is a weak function of virial mass, having the value $c \sim 5$ for masses characteristic of clusters. We can use this profile to relate the various mass definitions as shown in Fig. 3.

Unfortunately, while this model works well for converting between spherically averaged mass definitions based on M_Δ , there is a large scatter for masses based on group membership, such as $M_{\text{fof}0.2}$. This is because with $b = 0.2$, FOF can link together neighbouring haloes in supercluster-like structures, increasing the mass assigned to the structure compared to the M_Δ estimators. Thus the ‘FOF’ lines in Fig. 3 must be taken as highly uncertain. Comparing the mass function from a high-resolution N-body simulation (of the Ostriker & Steinhardt 1995 concordance model) with the universal form of Jenkins et al. (2000) we find the best match is obtained if we interpret their mass as M_{Δ_c} . We shall assume below that this remains true independent of cosmology. But we note that this ambiguity in the definition of mass remains a significant source of uncertainty.

2.5 The $M - T$ relation

The mass function of rich clusters is itself not observable. However the local temperature function is reasonably well known (see §3). To predict the latter from the former we need a relation between emission weighted IGM temperature and cluster virial mass. Our results are quite sensitive to the choice of $M - T$ relation, and currently the uncertainty in this relation is the largest theoretical source of error in determining σ_8 (see also Voit 2000).

Recent observational determinations of the mass-temperature relation (Horner, Mushotzky & Scharf 1999; Nevalainen, Markevitch & Forman 2000) disagree at the several tens of percent level (in mass at fixed temperature)

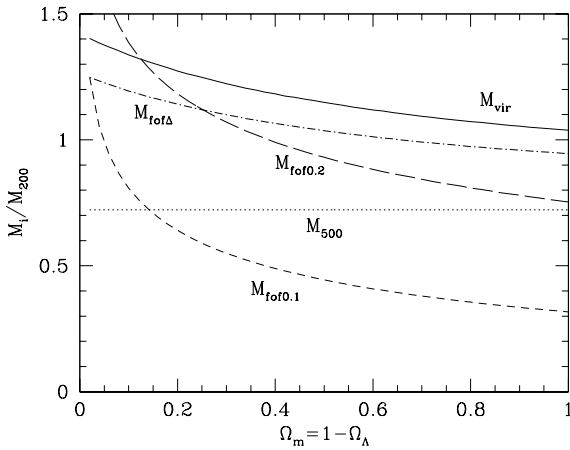


Figure 3. Relations between various definitions of the mass of a halo as a function of Ω_M assuming the halo density profile follows the NFW form with concentration parameter $c = 5$. The FOF based masses are only crude approximations in this model (see text).

when using different estimators of the cluster mass. The virial mass of a cluster is a notoriously difficult quantity to obtain observationally with high accuracy – while different estimators clearly correlate well, they disagree at the level of accuracy required here. Such observations do however provide general support for the functional form and scalings predicted by the spherical collapse model (see below) for clusters of sufficiently large mass. Similar scalings are seen in hydrodynamic simulations of galaxy clusters in a cosmological context. In the simulations the total mass of a cluster is easy to obtain (though convention dependent, §2.4) and in what follows we shall use a $M-T$ relation derived from simulations. While these hydrodynamic simulations show good agreement for the total mass and X-ray temperature properties of clusters (Frenk et al. 1999) there are several uncertainties which enter when comparing the simulations to observations and which are important to note.

As with all simulation derived results there are issues related to numerical convergence. With the latest round of high resolution simulations the situation in this respect has improved dramatically. However the spectrally measured cluster temperatures may not coincide with the mass or emission weighted temperature estimated from the simulations, due to the influence of soft line emission (Mathiesen & Evrard 2000). Secondly most simulations are done with purely adiabatic hydrodynamics, which ceases to be a good model for the lower mass/temperature clusters. It is also possible that energy injection (possibly from SNe, AGN or galaxies) has altered the $M-T$ relation, again an effect thought to operate preferentially on lower mass/temperature clusters. Thirdly the simulations usually predict the emission weighted temperature, which only converges if data are used out to a radius $\sim r_{500}$. Observers often probe different ranges of radius in determining the cluster temperature and perform more sophisticated modelling, which can lead to discrepancies between the measured and simulated temperatures. Finally, there still remain sig-

Name	Ω_M	Ω_Λ	Ω_B	h	β
EMN	1.0	0.0	0.10	0.50	1.21
EMN	0.2	—	0.10	0.50	1.42
ENF	0.3	0.7	0.04	0.70	1.33
BN	1.0	0.0	0.06	0.50	1.10
BN	1.0	0.0	0.10	0.65	1.04
BN	1.0	0.0	0.08	0.50	1.04
BN	0.4	0.0	0.06	0.65	1.08
YJS	0.3	0.7	0.03	0.70	1.48
TC*	1.0	0.0	0.10	0.65	1.61
Tetal*	1.0	0.0	0.06	—	1.23

Table 2. The mass-temperature relation determined from hydrodynamical simulations. The quoted value of β is that relevant for use in Eq. (13). In order of appearance the references are: EMN (Evrard et al. 1996); ENF (Eke et al. 1998); BN (Bryan & Norman 1998); YJS (Yoshikawa, Jing & Suto 2000); TC (Tittley & Couchman 2000) and Tetal (Thomas et al. 2000). We have quoted emission weighted temperatures where available, while the last two values (marked with an asterix) are core temperatures.

nificant (for our purposes) calibration uncertainties for the detectors.

With these caveats in mind, the results from the simulations can be quoted in terms of corrections to the spherical collapse model which relates the mass to the (virial) temperature of the hot IGM. For an object virialized at a redshift z we have[†]

$$\left(\frac{M(T, z)}{10^{15} h^{-1} M_\odot} \right) = \left(\frac{T}{\beta} \right)^{3/2} (\Delta_c E^2)^{-1/2} \times \left[1 - 2 \frac{\Omega_\Lambda(z)}{\Delta_c} \right]^{-3/2}, \quad (13)$$

where T is in keV, Δ_c is the mean overdensity inside the virial radius in units of the critical density and, from Eq. (4), $E^2 = \Omega_M(1+z)^3 + \Omega_\Lambda + \Omega_k(1+z)^2$. Note that Δ_c is a redshift dependent variable, and should be evaluated using the appropriate $\Omega_\Lambda(z)$ and $\Omega_M(z)$. The term in square brackets is a correction to the virial relation arising from the additional r^2 potential in the presence of Λ (Lahav et al. 1991; Viana & Liddle 1996; Wang & Steinhardt 1998). It provides only a small correction and, though we include it, it can be neglected at the present level of accuracy.

Ideally the normalization and scatter of the $M-T$ relation would be determined by simulations so that theoretical models can be compared with the data rather more directly (e.g. Pen 1998). However Eq. (13) is a remarkably good fit to the simulations, which are sufficiently computationally demanding that they cannot explore parameter space efficiently. Thus we rely on a hybrid approach where the coefficients are determined from simulations, while the scalings are taken from simple theoretical models (Mathiesen 2000). Specifically we use the hydrodynamic simulations to determine β , together with Eq. (13) for the mass and redshift dependence. In practice we used the $M-T$ relation at an

[†] Our definition of β differs from that of Henry (2000): $\beta_{\text{Henry}} = 1.42/\beta$.

observed $z = 0.053$, corresponding to the median redshift of our cluster sample (see §3). We then shift the resulting $\sigma(z = 0.053)$ value to $z = 0$ using the growth rate, Eq. (3), which is a significant 5 per cent correction.

The simulations normalize β assuming that the virialization redshift is the redshift of observation. In principle one could attempt to correct for the virialization redshift dependence, however we have chosen not to do this, and here we differ from Viana & Liddle (1999) and Wang & Steinhardt (1998), for example. The simulations, which clearly include the full effects of variations in the virialization redshift, give an $M-T$ relation well fit by Eq. (13) if z is interpreted as the redshift of observation. We believe that the effect of differing virialization redshifts is *included in the simulations as part of the scatter* about the mean relation (see below), and so to add an additional effect by hand would be incorrect. Comparison of the scatter in the $M-T$ relation found by Bryan & Norman (1998) in a full cosmological simulation with that of Evrard, Metzler & Navarro (1996) who use constrained realizations (and thus constrained formation times) suggests that in fact the effect of scatter in the virialization redshift is a very small source of the total scatter in the relation. While further simulations will be needed to address this issue properly, recent work (B.F. Mathiesen, in preparation) suggests that minor merger events have a more important influence on the evolution of the temperatures than major mergers (hence formation time).

A summary of recent numerical experiments which constrain β is given in Henry (2000). We have taken Henry's list, added some recent work and corrected one of the relations to use M_{vir} . Our results are shown in Table 2. The $M-T$ relation of Evrard et al. (1996) defines mass as M_{200} , so that in the context of the spherical top-hat model there is predicted to be an Ω_M dependence to the prefactor of the scaling relation. Correcting for this scaling brings the β s obtained in these simulations into better agreement, but they still disagree slightly, suggesting that the scaling is only approximately observed. We postulate that this is because Ω_B/Ω_M changes drastically between the simulations. The M s of Eke et al. (1998), Bryan & Norman (1998), and Yoshikawa et al. (2000), on the other hand, are already the 'virial' mass in the sense of the spherical top-hat model. Also quoted in Table 2 are the β values from Tittley & Couchman (2000) and Thomas et al. (2000). While all of the other temperatures in the Table are emission weighted, these authors use the average temperature within a core region, which could be slightly different.

As shown in Table 2 the values of β spread from near 1 up to 1.6 with no obvious peak of preferred values. We adopt the mean opinion on this issue, allowing for $\beta = 1.3$, with a 10 per cent systematic error (i.e. variation between the simulations) in the mass, plus a 10 per cent statistical error. The second error arises from the intrinsic scatter in individually determined $M-T$ relations, and is mostly due to the merging history of the clusters. Most of the simulations agree on the scatter about the mean relation quite well, though Eke et al. (1998) find a slightly enhanced scatter compared to the other authors. This dispersion is accurately modelled as a Gaussian, and we treat the systematic uncertainty as a Gaussian also. The β value advocated by Henry (2000) is slightly lower, $\beta = 1.17$, with a suggested systematic error

of 4.1 per cent, while the value we would obtain using the observational determinations is close to unity.

2.6 Summary of modelling

In summary we use the mass function of Jenkins et al. (2000), interpreting the mass as the top-hat virial mass. For an object at fixed mass we randomly assign a temperature using Eq. (13) where Δ_c is given by Eq. (10) and the $M-T$ relation is evaluated at a median redshift interpreted as the redshift of observation. From Table 2 we choose $\beta = 1.3 \pm 0.13 \pm 0.13$ with Gaussian errors. Here the first error represents the scatter about the mean relation and the second is the systematic uncertainty in the prefactor from the different calculations. We carry out the comparison between theory and data at the median redshift of the observations, and then correct the final normalization to the appropriate $z = 0$ value.

3 DATA

3.1 Definition of cluster sample

There has been progress recently in observationally determining the temperature function of nearby clusters, and we have compiled from the literature a new sample with which to constrain the normalization of the power spectrum at $z \simeq 0$.

The sample is adapted from the 30 clusters compiled by Markevitch (1998). His sample was selected from bright clusters having flux above $2 \times 10^{-14} \text{W m}^{-2}$ in the ROSAT 0.2–2 keV band, and over the redshift range $z = 0.04$ –0.09. The flux limit is a factor of 4 above the nominal flux limit of the ROSAT Brightest Cluster Sample (Ebeling et al. 1998), and hence the sample is expected to be close to complete for these fluxes. The upper redshift limit is imposed by the lack of clusters bright enough to be detected, and the lower limit by ROSAT selection effects. Clusters are also excluded with galactic latitude $|b| < 20^\circ$, where observations become affected by the Galaxy. This sample is close to volume limited at the high-temperature end, and the numbers can be corrected for incompleteness at the low-temperature end by using the effective volume (see §4.1). Markevitch (1998) determined temperatures by excising the central regions from clusters to approximately correct for the effects of cooling flows, and used a hybrid approach of combining ROSAT emissivity profiles with ASCA data to fit T_X . As we discuss below, we believe that somewhat better temperatures are now available based on careful fitting of ASCA data alone. Using mainly these temperatures, together with a somewhat different selection, we have attempted to define an *effectively temperature selected* sample.

White & Buote (2000) use a maximum likelihood method to determine radial temperature profiles for clusters using ASCA data alone. This includes a Monte Carlo method for redistribution of X-ray photons by ASCA's complex optics. They account for cooling flows using a single extra parameter in their fits, and find that the cooling flow corrected temperatures are generally consistent with what would be fitted to the outer regions of the clusters, although

with less uncertainty. They also do not find the temperature fall-off at large radii found by Markevitch (1998), about which there has been much discussion in the literature (e.g. Irwin, Bregman & Evrard 1999). We regard the temperatures presented in White (2000) as representing the most careful analysis of X-ray temperatures from available *ASCA* data. Independent *BeppoSAX* data, available for about a quarter of these clusters give temperatures in good agreement (Irwin & Bregman 2000). These values are unlikely to improve significantly until *Chandra* and *XMM-Newton* data become widely available.

We have constructed our cluster sample in a similar way to that given by Markevitch (1998), although we use temperatures from White (2000) when available, supplemented by other temperatures from the literature. The sample of course has a large overlap with other low-redshift cluster samples, such as those of Edge et al. (1990), Henry & Arnaud (1991), Henry (2000) and Blanchard et al. (2000) – although we neglect the lowest redshift clusters for reasons of incompleteness, as well as concerns about biases introduced by sample variance.

Since many of the White (2000) temperatures show significant changes compared with Markevitch (1998), we also need to reconsider the completeness of the sample. We use the estimated $L_X - T_X$ relationship derived from Markevitch (1998) to decide whether a cluster would be above the *ROSAT* flux limit based on the improved value of T_X . Since we find that the White (2000) temperatures are a factor $\simeq 1.14$ higher than the Markevitch (1998) temperatures on average for the clusters in common, we correct the $L_X - T_X$ relation by this factor. Explicitly we use

$$L_X = 1.07 \times 10^{37} \left(\frac{T_X}{6 \text{ keV}} \right)^{2.1} h^{-2} \text{W m}^{-2}, \quad (14)$$

where as usual $h = H_0/(100 \text{ km s}^{-1} \text{Mpc}^{-1})$. Markevitch (1998) finds a relatively small scatter about this relationship once cooling-flow effects have been corrected for. (A steeper temperature dependence is found for bolometric X-ray luminosity or luminosity over higher energy ranges.) The use of this relationship allows us to avoid using any specific *flux* information for a particular cluster, which is advantageous since this information is somewhat uncertain, varying significantly between instruments and between analysis methods. Provided Eq. (14) is approximately correct, the details will be a higher order correction to our σ_8 constraints.

Our sample is thus effectively *temperature*-selected at each redshift, and hence we will only need to correct for the volume sampled at each temperature over the full redshift interval. We use CMB-frame redshifts from the recent compilation of Struble & Rood (1999) for the Abell clusters, and the redshifts given in White (2000) or Ebeling et al. (1998) otherwise. At these low redshifts only a small error is made by assuming non-expanding Euclidean space, since the correction to the luminosity distance is $\mathcal{O}(z/4)$, which is ~ 2 per cent at worst. It is easy to compute the relationship exactly, although this would in principle have to be re-calculated for each model. We use redshift exactly as a distance indicator, which is another reason to cut off the sample at low redshifts, where this will cease to be a good approximation. The effective volume, as a function of temperature, is shown in Fig. 4. Because of the large com-

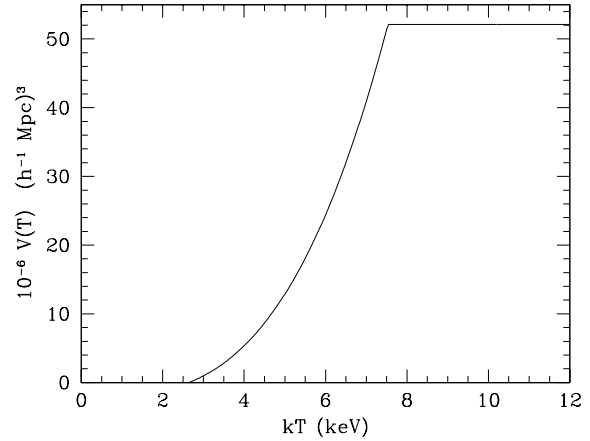


Figure 4. The effective volume of the sample as a function of temperature. Note that the sample is volume limited for clusters above about 7.5 keV, and that the correction factor is not too drastic for $kT \gtrsim 3.5$ keV.

pleteness correction required at low temperature, we make a further cut of all clusters with $T_X < 3.5$ keV. This also corresponds approximately to a restriction to clusters with temperatures which are dominated by gravitational physics (Mohr & Evrard 1997; Balogh et al. 1999; Xue & Wu 2000). Our final sample of 38 clusters is presented in Table 3.

3.2 Supplementary sample

Since we will be considering the temperature errors in our Monte Carlo error analysis (§4.2), some clusters will scatter out of the selection cuts and hence it is important to include clusters which could scatter *into* the sample. We include in Table 4 additional clusters with $T_X + 2\sigma$ being above our 3.5 keV cut-off, or above the temperature-derived flux limit at their redshift. This limit corresponds to

$$\frac{T_X}{\text{keV}} > 2.65 \left(\frac{z}{0.03} \right)^{0.95}, \quad (15)$$

and is indicated in Fig. 5 by the roughly diagonal line. To populate this supplementary sample (as well as to check completeness of the main sample) we extended the *ROSAT* selection down a further factor of 2 to $1.0 \times 10^{-14} \text{W m}^{-2}$. In particular we scrutinized the BCS sample of Ebeling et al. (1998), together with the RASS1 Bright Cluster Survey of (de Grandi et al. 1999) for the southern extension, and the overlapping XBACS sample came from either White (2000) or the David et al. (1993) compilation when available. For some clusters we used temperatures from the White, Jones & Forman (1997) deprojection modelling of *Einstein* data. For a few cases we had to resort to estimates (Ebeling et al. 1998) based on the X-ray luminosity – for those cases we adopted a representative error of ± 1.00 keV, which flags them in Table 3.

3.3 Comparison with other samples

Our final sample differs from that of (Markevitch 1998) in several details. We chose to widen the sample down to $z = 0.03$, since that increased the statistics, while we could find no evidence that there was any significant bias introduced. This can be seen in Fig. 5, where we have shown the clusters (solid points) together with our selection cuts in redshift and in temperature. Clusters which could scatter into our sample are indicated by open symbols.

The White (2000) temperatures were generally a little higher than those of Markevitch (1998), resulting in several clusters entering our sample, explicitly Abell 193, Abell 376, Abell 1775, Abell 2255, Abell 3532 and IIIZw108. On the other hand Abell 780, Abell 1650 and MKW3s were too cool at their redshifts, while Abell 3112 and 2A 0336 even failed the 2σ 3.5 keV cut. Abell 2199, Abell 2634 and Abell 4038, which are in some other samples, were lost here because their CMB-frame redshifts (Struble & Rood 1999) – as opposed to the heliocentric redshifts more commonly given – are slightly less than 0.03, while Abell 3921 is higher than 0.09. Furthermore we added Abell 496, Abell 576, Abell 2063, Abell 2107, Abell 2147, Abell 2151a, at $0.03 < z < 0.04$.

Our final sample of 38 clusters is presented in Table 3, where we list the common name, redshift (taken from Struble & Rood 1999 or White 2000), X-ray temperature and 1σ error bar. These are mostly from White (2000), but in a few cases from Markevitch (1998) errors scaled from 90 per cent confidence, or from the 80 per cent confidence region estimates of White et al. (1997). Table 4 lists the additional clusters which could scatter into our sample within their temperature uncertainties. Through this selection process we believe we have a reasonably constructed *temperature-selected* sample.

Though we do not use it directly in the analysis (see §4.1) we have constructed the temperature function of our sample for comparison with earlier work. We show this in Fig. 6, where we have only used the clusters in Table 3. Some of the other estimates plotted were derived for specific cosmological models or at other redshifts, so they cannot be compared in great detail. However, it is clear that we are in general agreement with the temperature function estimated by Markevitch (1998), although a little higher. More striking is that both of these estimates are considerably higher than those of Henry (2000) and of Eke et al. (1996) and Viana & Liddle (1999) which are based on the earlier Henry & Arnaud (1991) sample. The main reason for this difference is the correction for cooling flows. We believe that the most physically realistic comparison of the $z \simeq 0$ clusters with the results of simulations is to correct for cooling flows, since the full cooling-flow physics is not contained in the simulations. This gives rise to an added complication when carrying out evolutionary studies of the high- z vs low- z samples, since the high- z clusters tend not to contain cooling flows. However, for our purposes it seems clear that we should use cluster temperatures which have been corrected as carefully as possible for the effects of cooling flows.

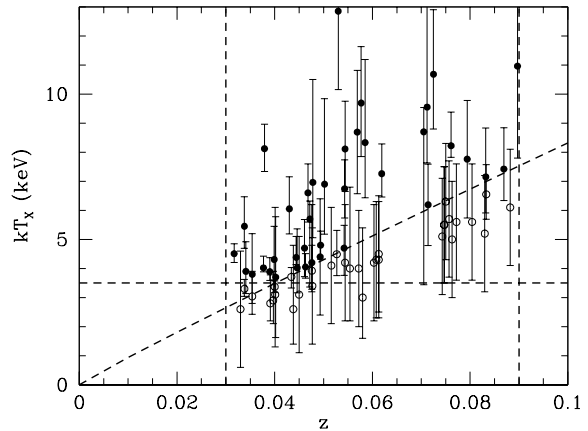


Figure 5. An indication of our selection function (dashed lines). We chose clusters (solid symbols) with CMB-frame redshifts within $0.03 < z < 0.09$ and a temperature-dependent function to account for a flux limit. We also cut out all clusters below $kT_X = 3.5$ keV. However, we kept clusters (shown as open circles) which could scatter into our acceptance region within their $\pm 2\sigma$ temperature uncertainties (which are plotted). Redshift errors are here assumed to be negligible. The lack of clusters at $z \simeq 0.065$ is a well-known effect caused by a genuine lack of superclusters at those distances.

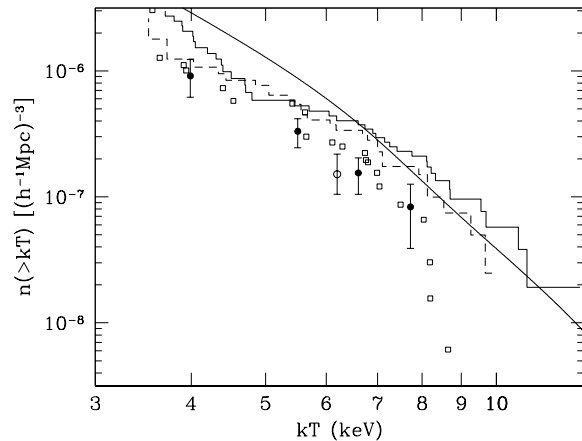


Figure 6. The temperature function constructed from the sample in Table 3 (solid line), compared to some earlier estimates. The dashed line is from Markevitch (1998), the boxes from Henry (2000), the filled circles from Eke et al. (1996), and the open circle from Viana & Liddle (1999). The dotted line is our best fit for a flat cosmology with $\Omega_M = 0.3$.

Name	z	T_X
A85	0.0543	$6.74^{+0.50}_{-0.50}$
A119	0.0430	$6.05^{+0.55}_{-0.43}$
A193	0.0476	$4.20^{+1.00}_{-0.50}$
A376	0.0472	$5.70^{+0.31}_{-0.31}$
A399	0.0712	$9.55^{+1.32}_{-0.96}$
A401	0.0725	$10.68^{+1.11}_{-0.94}$
A478	0.0869	$7.42^{+0.71}_{-0.54}$
A496	0.0317	$4.51^{+0.17}_{-0.15}$
A576	0.0377	$4.02^{+0.20}_{-0.07}$
A754	0.0530	$12.85^{+1.77}_{-1.35}$
A1644	0.0461	$4.70^{+0.49}_{-0.49}$
A1651	0.0832	$7.15^{+0.84}_{-0.62}$
A1736	0.0446	$4.02^{+0.67}_{-0.43}$
A1775	0.0705	$8.70^{+0.42}_{-2.63}$
A1795	0.0619	$7.26^{+0.51}_{-0.40}$
A2029	0.0761	$8.22^{+0.58}_{-0.20}$
A2063	0.0341	$3.90^{+0.51}_{-0.38}$
A2065	0.0714	$6.19^{+0.70}_{-0.70}$
A2107	0.0399	$4.31^{+0.57}_{-0.35}$
A2142	0.0897	$10.96^{+2.56}_{-1.58}$
A2147	0.0338	$5.45^{+0.51}_{-0.38}$
A2151a	0.0354	$3.80^{+0.70}_{-0.50}$
A2255	0.0794	$7.76^{+1.01}_{-1.01}$
A2256	0.0569	$8.69^{+1.06}_{-1.06}$
A2589	0.0402	$3.70^{+1.04}_{-1.04}$
A2657	0.0390	$3.89^{+0.24}_{-0.15}$
A3158	0.0585	$8.33^{+1.43}_{-0.95}$
A3266	0.0577	$9.69^{+0.97}_{-0.92}$
A3376	0.0444	$4.38^{+0.36}_{-0.12}$
A3391	0.0502	$6.90^{+1.47}_{-0.86}$
A3395	0.0494	$4.80^{+0.24}_{-0.24}$
A3532	0.0542	$4.70^{+0.39}_{-0.47}$
A3558	0.0468	$6.60^{+0.50}_{-0.50}$
A3562	0.0478	$6.96^{+1.77}_{-0.95}$
A3571	0.0379	$8.12^{+0.42}_{-0.39}$
A3667	0.0544	$8.11^{+0.82}_{-0.73}$
A4059	0.0463	$4.05^{+0.23}_{-0.19}$
IIZw108	0.0493	$4.40^{+1.00}_{-1.00}$

Table 3. Our nearby cluster sample. The data are adapted from the sample of Markevitch (1998) with White (2000) temperatures, and Struble & Rood (1999) redshifts, as discussed in the text. Reported errors are 1σ .

4 STATISTICAL APPROACH

4.1 The likelihood function

Rather than fitting to a measure of $n(>kT_X)$ at some fiducial T_X , we try to fit to all the data in a way which accounts for the Poisson distribution of clusters at each temperature using a likelihood method which takes full account of the errors. Our approach is similar to that of some other studies (e.g. Eke et al. 1996; Markevitch 1998; Henry 2000; Blanchard et al. 2000), but we describe it here in full, so that the differences can be appreciated.

Given a set of data with which to compare (§3) we compute the likelihood function for any given theory as follows. We break the range of temperatures under consideration

Name	z	T_X
A133	0.0554	$4.00^{+1.40}_{-0.90}$
A168	0.0438	$2.60^{+1.10}_{-0.60}$
A780	0.0527	$4.49^{+0.41}_{-0.37}$
A1650	0.0833	$6.55^{+0.51}_{-0.43}$
A1800	0.0743	$5.10^{+1.00}_{-1.00}$
A1831	0.0603	$4.20^{+1.00}_{-1.00}$
A2052	0.0338	$3.30^{+0.16}_{-0.13}$
A2061	0.0772	$5.60^{+1.00}_{-1.00}$
A2151	0.0354	$3.04^{+0.43}_{-0.31}$
A2249	0.0804	$5.60^{+1.00}_{-1.00}$
A2495	0.0763	$5.00^{+1.00}_{-1.00}$
A2572a	0.0391	$2.80^{+0.49}_{-0.30}$
A2593	0.0401	$3.10^{+1.50}_{-0.90}$
A2665	0.0544	$4.20^{+1.00}_{-1.00}$
A2734	0.0613	$4.50^{+1.00}_{-1.00}$
A3528a	0.0516	$4.10^{+1.00}_{-1.00}$
A3560	0.0477	$3.40^{+1.00}_{-1.00}$
A3695	0.0882	$6.10^{+1.00}_{-1.00}$
A3716	0.0450	$3.10^{+1.00}_{-1.00}$
A3809	0.0608	$4.30^{+1.00}_{-1.00}$
A3822	0.0747	$5.50^{+1.00}_{-1.00}$
A3822	0.0747	$5.50^{+1.00}_{-1.00}$
A3880	0.0572	$4.00^{+1.00}_{-1.00}$
EXO0422	0.0397	$2.90^{+0.50}_{-0.40}$
MKW3s	0.0434	$3.71^{+0.16}_{-0.19}$
RXJ1733	0.0330	$2.60^{+1.00}_{-1.00}$
S0405	0.0613	$4.30^{+1.00}_{-1.00}$
S1101	0.0580	$3.00^{+1.20}_{-0.70}$
SC1327	0.0476	$3.92^{+0.44}_{-0.32}$
Zw235	0.0830	$5.20^{+1.00}_{-1.00}$
Zw5029	0.0750	$6.30^{+1.00}_{-1.00}$
Zw8276	0.0757	$5.70^{+1.00}_{-1.00}$
Zw8852	0.0400	$3.37^{+0.10}_{-0.10}$

Table 4. Additional clusters which could scatter above our selection criteria within their $\pm 2\sigma$ temperature uncertainties. Additional temperatures come from David (1993) and White et al. (1997). Those with errors of ± 1.00 keV are estimates from X-ray luminosities.

into a large number of bins, chosen to be narrow enough so that the probability of two clusters occupying the same bin is very small. Then for a given Monte-Carlo realization (§4.2) of the temperatures of the set of clusters we place the clusters into the appropriate temperature bins, giving an occupation number $\eta_i = 0$ or 1 for each bin. For a predicted number density $\mathcal{N}_i = n(T)dT$, depending on our cosmological parameters, the mean occupation number of each bin is $\mu_i = \mathcal{N}_i V_i \ll 1$. Here V_i is the volume of space to which clusters in bin i can be seen:

$$V_i = \frac{\Omega_s}{3} (d_2^3 - d_1^3), \quad (16)$$

if the survey solid angle is Ω_s , which is $4\pi(1 - \cos 70^\circ) \simeq 8.27$ sr here. With a Euclidean assumption $d_1 = cz_1/H_0$, while

$$d_2 = \min \left(\frac{cz_2}{H_0}, \sqrt{\frac{L(T_X)}{4\pi f_{\text{lim}}}} \right), \quad (17)$$

where f_{lim} is the limiting flux of the survey ($2 \times 10^{14} \text{W m}^{-2}$) and $L(T_{\text{X}})$ is obtained from the luminosity-temperature relation, Eq. (14), given the cluster's temperature. Then the likelihood of observing this combination of clusters is simply

$$\ln \mathcal{L} = \sum_i [(\eta_i - 1)\mu_i + \eta_i(1 - \exp(-\mu_i))], \quad (18)$$

where by assumption only one of the two terms is non-zero for each bin i . This correctly accounts for the Poisson errors and uses the full temperature information from the sample.

4.2 Monte Carlos

Given that there are non-negligible uncertainties occurring in several places, that the calculation is quite non-linear, and that $n(T)$ is a steeply falling function, it is important to treat errors carefully. The only reasonable way to do this is through a Monte Carlo approach (also emphasized by Viana & Liddle 1999 and Blanchard et al. 2000), which we now describe. Firstly, we choose a temperature for each cluster (in Tables 3 and 4) by generating Gaussian random numbers, using the upper and lower error bars each 50 per cent of the time. Then we form a new sample by culling all clusters with temperatures which fail our selection cuts (as described in §3). Next we adopt a specific $M-T$ relation drawn from the central value and systematic range discussed in §2.5, together with an additional scatter, different for each temperature considered, arising from the intrinsic scatter in the $M-T$ relation. For each temperature, we use the M-T relation to calculate $n(T)$ according to the mass function in Eq. (8).

For each cosmological model considered, we then maximize the likelihood to find a best-fitting normalization from which to determine σ_8 . This whole process is repeated 1000 times to obtain a distribution of σ_8 values for each cosmology.

5 RESULTS

Our main result is the power spectrum normalization as a function of cosmological model. We quote the normalization for the variance on a scale R_{Cl} that corresponds to a cluster of 6.5 keV forming now. This is advantageous because the value of $\sigma(R_{\text{Cl}})$ is almost independent of the power-spectrum shape Γ (Blanchard et al. 2000), while at fixed $\sigma(R_{\text{Cl}})$ the value of σ_8 can vary by as much as 15 per cent as Γ spans the 68 per cent confidence range, 0.19–0.37, of Eisenstein & Zaldarriaga (2000). Fitting formulae accurate at the 1 per cent level for R_{Cl} and $\sigma(R_{\text{Cl}})$ in the range $0.2 \leq \Omega_M \leq 0.8$ and $0.3 \leq \Omega_\Lambda \leq 1$ are given by

$$R_{\text{Cl}} = \sum_{i,j=0}^3 d_{ij} x^i y^j \text{ h}^{-1} \text{Mpc}, \quad (19)$$

$$\sigma_{\text{Cl}} \equiv \sigma(R_{\text{Cl}}) = p_0 \Omega_M^{-(p_1 + p_2 \Omega_M + p_3 \Omega_\Lambda)}, \quad (20)$$

where $x \equiv \Omega_M - 0.2$, $y \equiv \Omega_\Lambda$ and the coefficients can be found in Tables 5 and 6. For $\sigma(R_{\text{Cl}})$ we also give fits to the $\pm 1\sigma$ limits in Table 6. For the concordance model ($\Omega_M = 0.3$) we find $R_{\text{Cl}} \simeq 15.6 \text{ h}^{-1} \text{Mpc}$, while for more general flat models a simpler fit is given by

i	0	1	2	3
j	0	1	2	3
0	18.6	-0.72	0.37	-0.03
1	-32.9	4.56	-3.57	1.47
2	54.3	-9.76	9.29	-4.47
3	-37.4	6.93	-7.09	3.51

Table 5. Coefficients d_{ij} of the fitting formula, Eq. (19), for the normalization scale $R_{\text{Cl}} = \sum_{i,j=0}^3 d_{ij} x^i y^j h^{-1} \text{Mpc}$, with $x \equiv \Omega_M - 0.2$, $y \equiv \Omega_\Lambda$.

	parameter			
	p_0	p_1	p_2	p_3
mean	0.508	0.187	-0.286	0.011
-1σ	0.475	0.166	-0.285	0.013
$+1\sigma$	0.533	0.203	-0.261	0.012

Table 6. Coefficients of the fitting formula, Eq. (20), for the mean and errors of $\sigma(R_{\text{Cl}}) = p_0 \Omega_M^{-(p_1 + p_2 \Omega_M + p_3 \Omega_\Lambda)}$.

$$R_{\text{Cl}} \simeq 9.54 \Omega_M^{-0.41} h^{-1} \text{Mpc}. \quad (21)$$

This fits to better than 1 per cent over $0.2 \leq \Omega_M \leq 0.8$.

For explicit constraints on σ_8 we verified that the following equation is a good fit with a maximum error of 2 per cent, in the range $0.19 \leq \Gamma \leq 0.37$ (Eisenstein & Zaldarriaga 2000), $0.2 \leq \Omega_M \leq 0.8$ and $0.3 \leq \Omega_\Lambda \leq 1$:

$$\sigma_8 = \sigma_{\text{Cl}} q_0 \Omega_\Lambda^{q_1} \Omega_M^{-(q_2 + q_3 \Omega_M)} \Gamma^{(q_4 + q_5 \Omega_M)}. \quad (22)$$

Here the vector of coefficients is given by $\vec{q} = (1.107, -0.002, 0.559, 0.341, 0.287, -0.292)$. For flat models (i.e. $\Omega_\Lambda = 1 - \Omega_M$) this corresponds approximately to

$$\sigma_8 \simeq (0.495_{-0.037}^{+0.034}) \Omega_M^{-0.60} \quad (23)$$

for $\Gamma = 0.23$ explicitly, and for general Γ :

$$\sigma_{\text{Cl}} = 0.462_{-0.029}^{+0.027} \Omega_M^{-0.194 \{ -0.179 \}_{-0.218}}, \quad (24)$$

where the exponents in brackets refer to the best power-laws for the $+1\sigma$ and -1σ limits.

We performed several checks on our results. First we made sure that analysing the sample using a single (median) redshift did not introduce a significant bias. We split the sample into low- z and high- z halves and analysed them independently. The variation in σ_{Cl} between the low- z , high- z and combined samples was only 2 per cent for a flat model with $\Omega_M = 0.3$. We also gradually eliminated clusters with redshift below a threshold z_* , and then above that threshold. The results change smoothly with z_* , implying that the final result is not dominated by any particular cluster. Finally we eliminated all clusters below 6 keV (which approximately halves the sample in each Monte-Carlo realization). While the errors increase in this process, the central value only increases by 3–5 per cent (depending on Ω_M).

In earlier cluster samples the shape of the temperature function was not obviously well fit by the theoretical predictions. Much of this discrepancy has now disappeared thanks to better data. The question remains however as to how much the shape of the temperature function affects the fit,

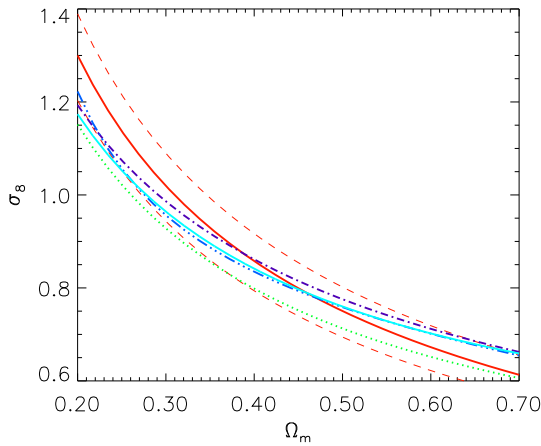


Figure 7. The normalization σ_8 for flat cosmologies with $\Gamma = 0.23$ as derived here (solid red line) with $1-\sigma$ limits (dashed red lines) compared with the results of Viana & Liddle (1999) (purple, dot-dashed line), Wang & Steinhardt (1998) (blue, 3 dots-dashed), Eke et al. (1996) (green, dotted), Borgani et al. (1999) (cyan, long dashed).

rather than for example the overall amplitude at some intermediate temperature. To address this we have calculated σ_{Cl} for flat cosmologies by matching the observed $n(>kT_X)$ for $T_X = 6 \text{ keV}$. We found values 2.5–4.5 per cent lower than fitting to the whole temperature function for $T_X > 3.5 \text{ keV}$. Since fitting the whole temperature function above 6 keV would imply an increase of 3–5 per cent, we can conclude that the shape of the temperature function is an important consideration at the required level of accuracy.

In Fig. 7 we compare our results with those of Viana & Liddle (1999) for flat cosmologies as a function of Ω_M .[†] While the Viana & Liddle (1999) best fit is within our error bars, the shape of the two curves is quite different. This discrepancy can be traced to a number of factors: a newer data compilation; our likelihood fit to the entire cluster data; our use of the Sheth & Tormen (1999) universal mass function rather than the PS theory; not integrating over formation redshifts; different $M-T$ normalization and scatter; and different sources of errors (in particular Viana & Liddle 1999 included errors in Γ).

We found a relatively symmetric error bar on our final results for σ_{Cl} and σ_8 , while Viana & Liddle (1999) had a very asymmetric error. It appears that this is mainly due to the assumed skew distribution for Γ . Another important difference is that Viana & Liddle (1999) adopted a lower value of β with respect to ours. If we chose $\beta = 1.17$, we would find the same normalization at high Ω_M (see Fig. 8). Approximately half of the discrepancy at lower Ω_M comes from the fact that we have not integrated over ‘formation’

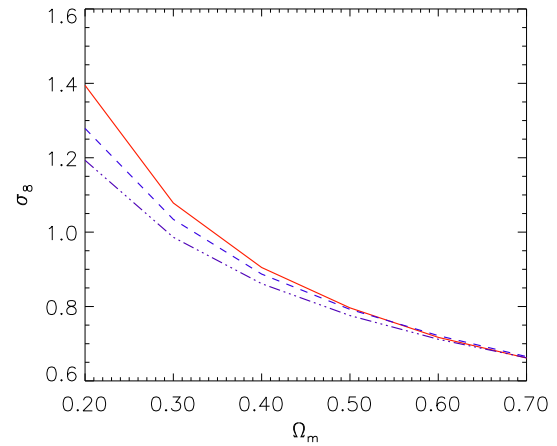


Figure 8. The normalization σ_8 for flat cosmologies with $\Gamma = 0.23$ as derived here (solid red line) compared with the Viana & Liddle (1999) results (purple, dot-dashed line) and with their approach but without the integration over formation redshift (blue, dashed line).

redshift, while Viana & Liddle (1999) included such an integration (see Fig. 8). We argued in §2 that including such an integration in addition to the scatter in the $M-T$ relation was effectively double counting some of the scatter.

Use of the Sheth & Tormen (1999) or Jenkins et al. (2000) mass function, rather than PS, *lowers* our results by 4–8 per cent (depending on Ω_M). Note that the overall effect of the different mass function may depend on redshift, so that if formation redshift is integrated over then the discrepancy may even be in the other direction.

A major source of theoretical uncertainty remains the value and distribution of β in the $M-T$ relation of Eq. (13). We show in Fig. 9 how σ_{Cl} changes as β is scanned from 0.9 to 1.5 (with no systematic error) in our reference model with $\Omega_M = 0.3$ and $\Omega_\Lambda = 0.7$. It is clear that a better estimate of the $M-T$ relation would greatly reduce the errors, but the actual uncertainties on β would imply a very much different σ_{Cl} value, rendering the introduction of the systematic error essential.

An estimate of the uncertainty introduced by various factors is shown in Table 7. To obtain the estimates of error budget in this table we ran our code with the sources of errors described in the first column. The first case for example is the complete calculation, with all sources of error included. The second case has only the statistical uncertainty in the $M-T$ relation, while the uncertainty in the value of the cluster temperature and the systematic scatter in the $M-T$ relation were not used. The other cases show what happens with one or other source of uncertainty excluded. The mean quoted is the mean of the distribution obtained in each case, while the errors are obtained by integrating the normalized distribution until 34 per cent of the area is reached on each side of the mean.

We find that our uncertainty in σ_8 is dominated by systematics in the $M-T$ relation (see also Voit 2000). The statistical scatter in the $M-T$ relation has an almost negligible

[†] Many authors have found similar results which differ slightly from Viana & Liddle. We choose their study for detailed comparison, since they were very explicit about the details of their procedure. See Wang & Steinhardt (1998) for a detailed discussion of differences between some other studies.

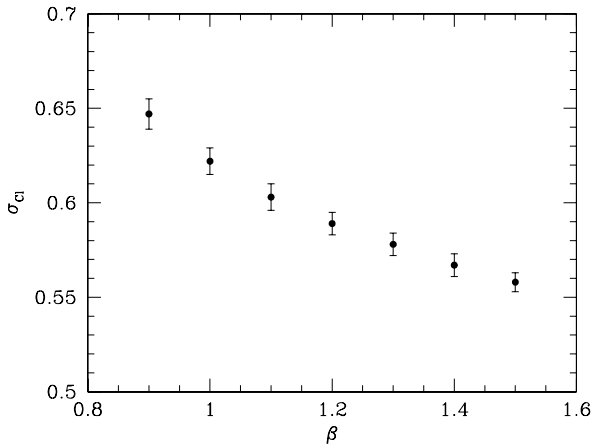


Figure 9. The largely Γ -independent normalization $\sigma(R_{CI})$ for different values of β in the $M-T$ relation. The error bars indicate the standard deviation of $\sigma(R_{CI})$ arising from all uncertainties except for the systematic error in β , which is set to zero. Our adopted central value of β is 1.3.

Source of error	mean $\sigma(R_{CI})$	$+1\sigma$	-1σ
all	0.581	0.049	0.050
$M-T _{\text{sys}}$	0.575	0.047	0.047
$M-T _{\text{stat}}$	0.570	0.002	0.002
T	0.586	0.005	0.018

Table 7. For a flat cosmology with $\Omega_M = 0.3$ we estimate how each source of uncertainty affects the mean and the error of our σ_{CI} estimates. $M-T|_{\text{sys}}$ and $M-T|_{\text{stat}}$ represent the systematic and statistical errors in the $M-T$ relation, while T represents the error in the temperature of the clusters. The $+1\sigma$ and -1σ limits are found from integrating the distribution of 1000 Monte Carlos in each case.

effect on the central value and the error. The temperature errors themselves give a skewed distribution to σ_8 , but this effect is sub-dominant.

6 CONCLUSIONS

The local abundance of rich clusters of galaxies currently provides one of the strongest constraints on the normalization of the present day dark matter power spectrum on a scale of ~ 10 Mpc. While there have been numerous detailed studies of this constraint in the past, recent developments in both theory and observation have made it worthwhile to revisit this quantity.

We have calculated the constraint on σ_8 arising from a new local sample of X-ray clusters with *ASCA* temperatures. We have incorporated the universal mass function determined from recent large N-body simulations, which is sufficiently different from the PS theory that the cosmological constraints inferred from cluster abundances change. We tried to carefully define the relation between mass and X-ray temperature for galaxy clusters, based on the results of many different hydrodynamical simulations. Another major

difference with previous work was that we performed all the comparisons at the ‘observed epoch’ rather than carrying out an integration over ‘formation times’. We also considered general combinations of Ω_M and Ω_Λ , including closed models. Our results are best presented in terms of a normalization at the scale for our sample, R_{CI} , where the normalization is largely independent of the power spectrum shape.

In the near future we anticipate a dramatic increase in our knowledge of the cosmological parameters from CMB anisotropy missions. In particular it has been forecast (Eisenstein, Hu & Tegmark 1999) that *MAP* will be able to determine σ_8 to 14 per cent, at the same time as constraining a suite of other parameters. The cluster abundance constraint is currently uncertain only at the ~ 10 per cent level, and so certainly is a pivotal limit on models – it is also an entirely independent constraint (at low z , in the mildly non-linear regime) compared with the CMB determinations (derived from the purely linear regime at $z \simeq 1000$). The uncertainty in the derived σ_8 could be dramatically reduced with improvement in the $M-T$ relation, as well as through new X-ray data coming from *Chandra* and *XMM-Newton*.

Future X-ray surveys, which go much fainter will lead to an increase in the size and quality of the X-ray data. We showed in Fig. 4 that there is lots of volume that was not probed at, say, 5 keV. For example the *ROSAT* Bright Survey (Schwope et al. 2000) contains an approximately complete flux-limited sample of 302 clusters at $|b| > 30^\circ$, most of them lying at low redshift, which would be an excellent database if they all had good temperature estimates. More important than just increasing the precision of the X-ray temperature measurements is an increase in the quality of data, for the purposes of more fully understanding the comparison with models. Better spatial and spectral information from X-ray clusters should allow more reliable estimates for the value of T_X which is most appropriate for comparing with the simulations. In a similar vein, improved optical studies of lensing and velocity dispersions could improve mass determinations for individual clusters.

The major improvement will come through a more precise mass-temperature relation for X-ray clusters. This will require both the improved data which we can foresee from *Chandra* and *XMM-Newton*, and improvements in modelling the gas physics relevant for understanding the X-ray properties of clusters. Eventually we imagine that the data will be fit more directly to much more ambitious simulations – this will be extremely difficult in practice, since a wide range of scales needs to be modelled simultaneously. In the meantime the piece-meal approach we have taken here will continue to be useful. And with each of the ingredients, particularly the mass-temperature relation, improving with time, the cluster abundance will continue to be a strong constraint on the normalization of dark matter fluctuations on the ~ 10 Mpc scale.

ACKNOWLEDGMENTS

EP and DS were supported by the Canadian Natural Sciences and Engineering Research Council, and MW by the US National Science Foundation and a Sloan Fellowship. EP is a National Fellow of the Canadian Institute for Theoretical Astrophysics. We would like to thank the Institute

for Theoretical Physics for their hospitality while some of this work was carried out, and Stefano Borgani for useful comments. This research has made use of the NASA/IPAC Extragalactic Database (NED) which is operated by the Jet Propulsion Laboratory, California Institute of Technology, under contract with the National Aeronautics and Space Administration.

REFERENCES

Allen S.W., 1998, MNRAS, 296, 392
 Bahcall N., Cen R., 1993, ApJ, 407, L49
 Balogh M.L., Babul A., Patton D.R., 1999, MNRAS, 307, 463
 Bardeen J.M., Bond J.R., Kaiser N., Szalay A.S., 1986, ApJ, 304, 15
 Blanchard A., Sadat R., Bartlett J.G., Le Dour M., 2000, preprint [astro-ph/9908037]
 Bond J.R., Myers S.T., 1991, Trends in Astroparticle Physics, eds. D. Cline, R. Peccei, World Scientific, Singapore, p. 262
 Bond J.R., Myers S.T., 1996, ApJS, 103, 63
 Borgani S., Rosati P., Tozzi P., Norman C., 1999, ApJ, 517, 40
 Bryan G.L., Norman M.L., 1998, ApJ, 495, 80
 Cohn J., 1999, Astrophys. & Space Science, 259, 213.
 Carroll S.M., Press W.H., Turner E.L., ARAA, 30, 499
 Carroll S.M., 2000, Living Review in Relativity [astro-ph/0004075]
 Cavaliere A., Menci N., Tozzi P., 1999, MNRAS, 308, 599
 Colafrancesco S., Mazzotta P., Vittorio N., 1997, ApJ, 488, 566
 David L.P., Slyz A., Jones C., Forman W., Vrtilek S.D., et al. 1993, ApJ, 412, 479
 Davis M., Efstathiou G., Frenk C.S., White S.D.M., 1985, ApJ, 292, 371
 de Grandi S., Böhringer H., Guzzo L., Molendi S., Chincarini G., et al. 1999, ApJ, 514, 148
 Ebeling H., Voges W., Böhringer H., Edge A.C., Huchra J.P., et al. 1996, MNRAS, 281, 799
 Ebeling H., Edge A.C., Böhringer H., Allen S.W., Crawford C.S., et al. 1998, MNRAS, 301, 881
 Edge A., Stewart G.C., Fabian A.C., Arnaud K.A., 1990, MNRAS, 245, 559
 Eisenstein D., Hu W., 1999, ApJ, 511, 5
 Eisenstein D., Hu W., Tegmark M., 1999, preprint [astro-ph/9807130]
 Eisenstein D., Zaldarriaga M., 2000, preprint [astro-ph/9912149]
 Eke V., Cole S., Frenk C.S., 1996, MNRAS, 282, 263
 Eke V., Cole S., Frenk C.S., Henry P.J., 1998, MNRAS, 298, 1145
 Eke V., Navarro J.F., Frenk C.S., 1998, ApJ, 503, 569
 Evrard A.E., 1989, ApJ, 341, L71
 Evrard A.E., Metzler C., Navarro J.F., 1996, ApJ, 469, 494
 Finoguenov A., Arnaud M., David L.P., 2000, ApJ, submitted [astro-ph/0009007]
 Frenk C.S., White S.D.M., Efstathiou G., Davis M., 1990, ApJ, 351, 10
 Frenk C.S., White S.D.M., Bode P., Bond J.R., Bryan G.L., et al. 1999, ApJ, 525, 554
 Gardner J.P., 2000, preprint [astro-ph/0006342]
 Girardi M., Giuricin G., Mardirossian F., Mezzetti M., Boschin W., 1998, ApJ, 505, 74
 Girardi M., Borgani S., Giuricin G., Mardirossian F., Mezzetti M., 1998, ApJ, 506, 45
 Governato F., Babul A., Quinn T., Tozzi P., Baugh C.M., et al., 1999, MNRAS, 307, 949
 Hamilton A.J.S., 2000, submitted to MNRAS [astro-ph/0006089]
 Hanami H., 1993, ApJ, 415, 42
 Heath D.J., 1977, MNRAS, 179, 351
 Henry J.P., 2000, ApJ, in press [astro-ph/0002365]
 Henry J.P., Arnaud K.A., 1991, ApJ, 372, 410
 Horner D.J., Mushotzky R.F., Scharf C.A., 1999, ApJ, 520, 78
 Irwin J.A., Bregman J.N., 2000, ApJ, in press [astro-ph/0003123]
 Irwin J.A., Bregman J.N., Evrard A.A., 1999, ApJ, 519, 518
 Jenkins A., Frenk C.S., White S.D.M., Colberg J.M., Cole S., Evrard A.E., Yoshida N., 2000, MNRAS, in press [astro-ph/0005260]
 Kaiser N., 1991, ApJ, 383, 104
 Kitayama T., Suto Y., 1997, ApJ, 490, 557
 Lahav O., Rees M.J., Lilje P.B., Primack J.R., 1991, MNRAS, 251, 128
 Liddle A., Lyth D., 2000, Cosmological Inflation and Large-Scale Structure, Cambridge University Press, Cambridge.
 Lilje P.B., 1992, ApJ, 386, L33
 Markevitch M., 1998, ApJ, 504, 27
 Mathiesen & Evrard, 2000, preprint [astro-ph/0004309]
 Mathiesen B.F., 2000, in preparation
 Mohr J.J., Evrard A.E., 1997, ApJ, 491, 38
 Molnar S.M., Jahoda K., 2000, [astro-ph/0002270]
 Navarro J.F., Frenk C.S., White S.D.M., 1996, ApJ, 462, 563
 Nevalainen J., Markevitch M., Forman W., 2000, ApJ, in press [astro-ph/9911369]
 Ostriker J.P., Steinhardt P.S., 1995, Nature, 377, 600
 Oukbir J., Blanchard A., 1992, A&A, 262, L21
 Peacock J.A., 1999, Cosmological Physics, Cambridge University Press, Cambridge.
 Peebles, P.J.E., 1993, Principles of Physical Cosmology, Princeton University Press, Princeton, chapter 25.
 Pen U.-L., 1998, ApJ, 504, 601
 Press W.H., Schechter P., 1974, ApJ, 187, 452
 Reiprich T.H., Böhringer H., 1999, preprint [astro-ph/9908357]
 Schwope A.D., Hasinger G., Lehmann I., Schwarz R., Brunner H. et al. 2000, Astron. Nach., 321, 1
 Sheth R.K., Mo H.J., Tormen G., 2000, MNRAS, in press [astro-ph/9907024]
 Sheth R.K., Tormen G., 1999, MNRAS, 308, 119
 Struble M.F., Rood H., 1999, ApJS, 125, 35
 Tanaka Y., Inoue H., Holt S.S., 1994, PASJ, 46, L37
 Thomas P.A., Muanwong O., Pearce F.R., Couchman H.M.P., Edge A.C., et al., submitted to MNRAS [astro-ph/0007348]
 Tittley E.R., Couchman H.M.P., 2000, submitted to MNRAS [astro-ph/9911365]
 Viana P.T.P., Liddle A., 1996, MNRAS, 281, 323
 Viana P.T.P., Liddle A., 1999, MNRAS, 303, 535
 Voit G.M., 2000, ApJ, in press [astro-ph/0006366]
 Wang L., Steinhardt P.J., 1998, ApJ, 508, 483
 White D.A., 2000, MNRAS, in press [astro-ph/9909467]
 White D.A., Buote D.A., 2000, MNRAS, 312, 649
 White D.A., Jones C., Forman W., 1997, MNRAS, 292, 419
 White M., Scott D., 1996, ApJ, 459, 415
 White M., Scott D., Pierpaoli E., 2000, ApJ, in press
 White S.D.M., Efstathiou G., Frenk C.S., 1993, MNRAS, 262, 1023
 Xue Y.-J., Wu X.-P., 2000, ApJ, 538, 65
 Yoshikawa K., Jing Y.P., Suto Y., 2000, ApJ, in press [astro-ph/0001076]